ACS Macro Letters

pubs.acs.org/macroletters Letter

Unraveling the Unconventional Order of a High-Mobility Indacenodithiophene–Benzothiadiazole Copolymer

Camila Cendra, Luke Balhorn, Weimin Zhang, Kathryn O'Hara, Karsten Bruening, Christopher J. Tassone, Hans-Georg Steinrück, Mengning Liang, Michael F. Toney, Iain McCulloch, Michael L. Chabinyc, Alberto Salleo,* and Christopher J. Takacs*

Cite This: *ACS Macro Lett.* 2021, 10, 1306–1314 Read Online

ACCESS | Metrics & More | Article Recommendations | Supporting Information

ABSTRACT: A new class of donor–acceptor (D–A) copolymers found to produce high charge carrier mobilities competitive with amorphous silicon (>1 cm^2 V^{-1} s^{-1}) exhibit the puzzling microstructure of substantial local order, however lacking long-range order and crystallinity previously deemed necessary for achieving high mobility. Here, we demonstrate the application of low-dose transmission electron microscopy to image and quantify the nanoscale and mesoscale organization of an archetypal D–A copolymer across areas comparable to electronic devices (≈9 μm^2). The local structure is spatially resolved by mapping the backbone (001) spacing reflection, revealing nanocrystallites of aligned polymer chains throughout nearly the entire film. Analysis of the nanoscale structure of its ordered domains suggests significant short- and medium-range order and preferential grain boundary orientations. Moreover, we provide insights into the rich, interconnected mesoscale organization of this new family of D–A copolymers by analysis of the local orientational spatial autocorrelations.

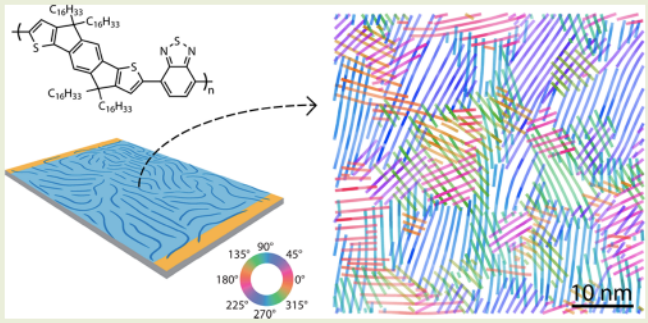

Due to their solution processability, flexibility, and synthetic tunability, conjugated polymers (CPs) have emerged as promising materials for solar cells,[1] flexible displays,[2] energy storage,[3] chemical sensors,[4] neural probes,[5] and neuromorphic computing.[6] In all of these applications, the functionality and performance depend strongly on the solid-state molecular and mesoscale organization.[7−9] Charge transport requires continuous electronic coupling across all length scales (i.e., atomic to mesoscale) and consideration of anisotropies at the molecular level.[10,11] There are notable examples of higher-order mesoscale organization and molecular packing structures in polymeric systems; however, their discovery is often serendipitous, and their roles are poorly understood.[12−27] A grand challenge in this area of materials science is to uncover how molecular structure and processing produce the hierarchal solid-state structures that ultimately govern materials properties, be they optoelectronic, electrochemical, or even mechanical. Indeed, a detailed understanding of the morphology has remained elusive in CPs, largely due to the difficulty to capture intricate, complex, and heterogeneous structures using typical materials science characterization techniques such as electron microscopy and X-ray scattering.

Several well-performing donor–acceptor (D–A) copolymers described as structurally "disordered" owing to lack of conventional long-range crystalline order exhibit large persistence lengths.[28−30] This extended structure along the backbone direction and efficient charge transport suggest short-to-medium range nanometer-scale structural organization is likely both present and important. Assessing their extent of ordering at short- and medium-range length scales (i.e., nearest neighbors, next-nearest neighbors, and beyond, respectively) is imperative toward a complete picture of structural heterogeneity. Low-dose transmission electron microscopy (TEM) has proven to be a viable approach to characterize the local and intercrystallite order of CP thin films from the atomic to mesoscopic scales.[14,15,24,26,31−40] In glassy materials, TEM techniques have revealed nanometer-scale ordered clusters in a more disordered matrix.[34,41−43] Beyond direct damage, electron-beam/materials interactions have several other practical consequences on TEM image contrast. These include contrast reduction through damage-induced mechanical strain/vibrations and charge fluctuations within the sample that blur image contrast.[44] With the introduction of active-pixel-counting electron detectors, dose-fractionated TEM image stacks under low-dose conditions offer the potential to address

Received: August 21, 2021
Accepted: September 27, 2021
Published: October 5, 2021

https://doi.org/10.1021/acsmacrolett.1c00547
ACS Macro Lett. 2021, 10, 1306–1314

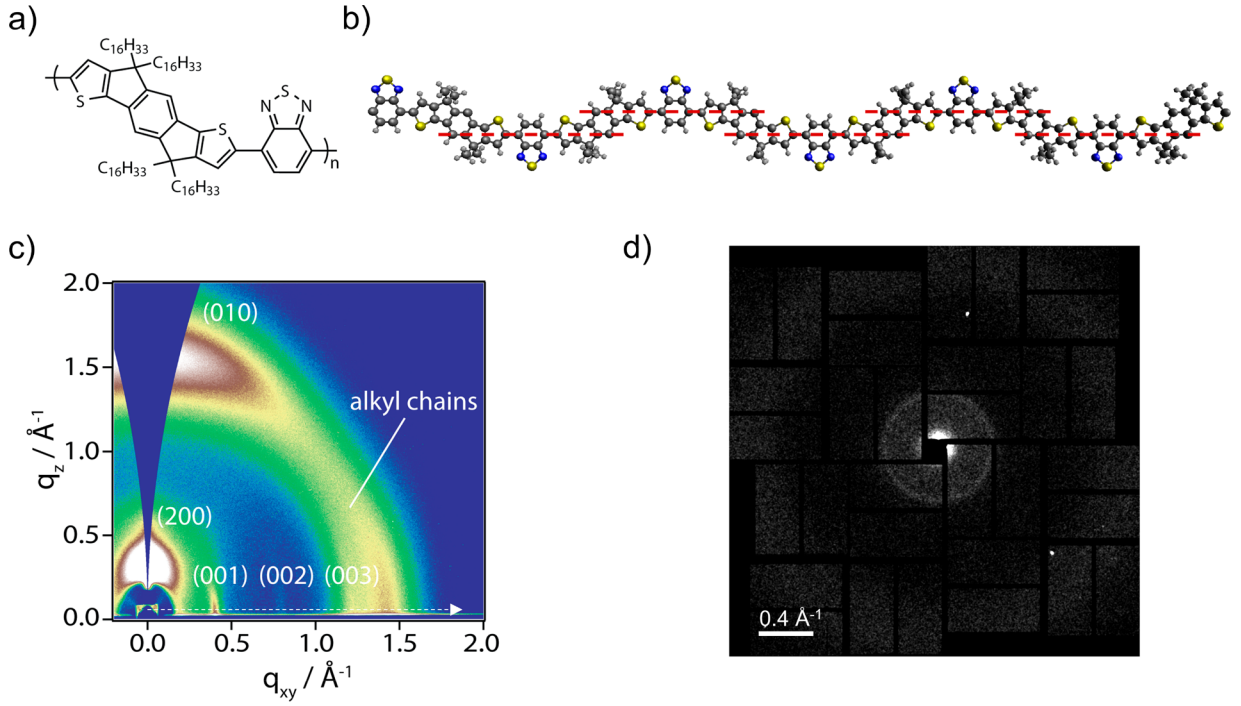

Figure 1. Molecular structure and packing properties of IDT-BT. (a) Chemical structure. (b) Optimized gas-phase geometry with side chains omitted. The acceptor (IDT) block appears to wander; however, the entrance and exit angle of each monomer is nearly colinear. Thus, in a long chain, a cis configuration tends to offset the chain slightly (red dashed lines) but does not radically change its direction. (c) 2D GIWAXS pattern. Dashed arrow denotes in-plane scattering direction. (d) Single-shot FEL X-ray diffraction pattern (in transmission mode) using a nanofocus beam. The estimated beam size is ≈250 nm at full width at half-maximum.

and correct these contrast issues to improve imaging resolution and signal-to-noise ratio.[45]

Here, we present an approach to low-dose, high-resolution TEM (HRTEM) that takes advantage of the many instrumental advances developed to study biological specimens[46] to reveal previously undetected structural features. Specifically, we detect a surprising degree of short- and medium-range order in a high-performance indacenodithiophene-*co*-benzothiadiazole copolymer (IDT-BT) whose microstructure is commonly referred to as "amorphous-like" based on its broad, weak X-ray diffraction.[47] Analysis reveals the presence of locally aligned regions of polymer chains throughout the entirety of the sample with frequent overlaps of the domains. We leverage the vast amount of available information to describe and quantify higher-order structural relationships across various length scales. First, we identify and segment self-similar regions exhibiting alignment to estimate the size distribution of nanoscale domains and examine the nature of short- and medium-range order. Second, we examine the rich, interconnected mesoscale organization of IDT-BT through estimation of the local orientational correlations. The results agree with complementary synchrotron and free-electron laser (FEL) hard X-ray characterization. Our results exemplify the applicability of using low-dose HRTEM imaging and cryo-EM-inspired analysis methods to characterize the nano- and mesoscale organization of IDT-BT, which is essential for further understanding the role of structure in a new class of high-performing CPs lacking pronounced long-range order.

Initially described by Zhang et al.,[48] IDT-BT (Figure 1a) is a prominent example of a new class of D−A copolymers lacking pronounced long-range order,[29,47] yet displaying remarkable optoelectronic properties and high charge carrier mobilities (2−10 cm^2 V^{-1} s^{-1}).[49,50] These properties were attributed to nearly planar, torsion-free backbone conformations[51] and low degrees of energetic disorder,[49] with recent evidence suggesting the formation of excitons at close-crossing points where chains aggregate strongly.[52,53]

The alkyl side chains influence solid-state macromolecular order and play a critical role in the self-assembly process.[54] In IDT-BT, the long alkyl side chains are likely disordered, creating regions of excluded volume around the planar backbones that can extend above and below the rigid plane of the backbone. Moreover, at the level of a single IDT unit, there is a local inversion symmetry where the side chains attach that could create significant steric hindrances. The backbone is thought to be both highly planar and linear (Figure S1).[49,51,55] Importantly, rotations along the chain have unusual consequences since the monomer entrance and exit angles are approximately colinear and offset (Figure 1b). As a result, in thin films, the molecular structure of IDT-BT along the backbone direction is likely to present various conformational isomers that maintain a rigid, planar rod topology. Thus, the chain direction may wander but is not expected to bend the chain strongly, resulting in an entropically linear/rod-like chain.[56] Combined with the sterically encumbered and unusual local symmetry of the IDT unit in the monomer, we expect a range of complex and potentially unconventional morphologies may be present in the solid state. Here, ≈40 nm IDT-BT samples were prepared via spin coating (1500 rpm, 60 s) from chloroform (5 mg mL^{-1}) onto silicon/SiO_2 substrates (Section 1, SI).

The bulk packing characteristics of IDT-BT as probed by grazing-incidence wide-angle X-ray scattering (GIWAXS) agree with the literature (Figure 1c and Figure S2),[47,48] where the most prominent feature is a single family of sharp in-

https://doi.org/10.1021/acsmacrolett.1c00547
ACS Macro Lett. 2021, 10, 1306−1314

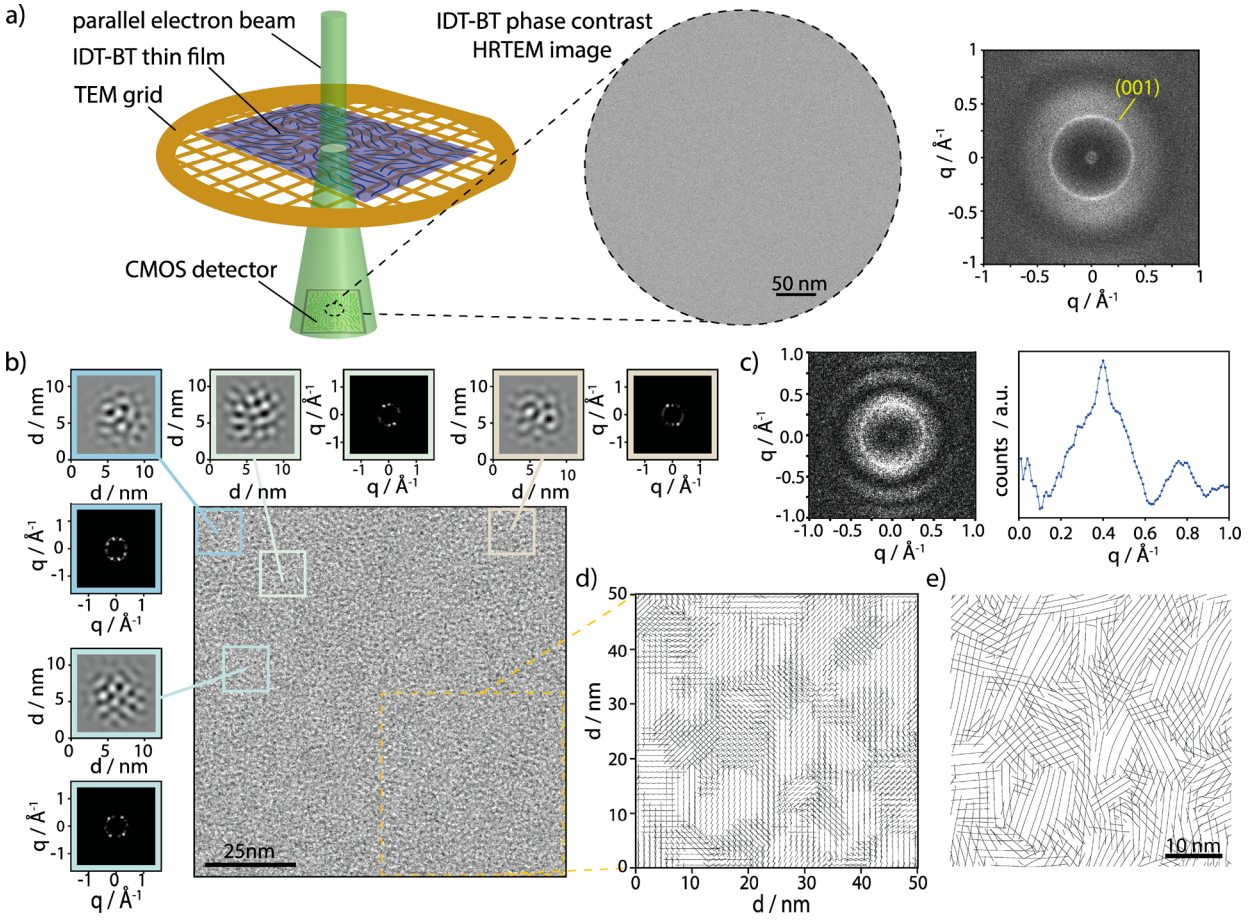

Figure 2. Visualization of nanoscale ordering along the backbone direction in IDT-BT. (a) Schematic of the HRTEM imaging process (left), a phase contrast HRTEM image of a 0.125 μm^2 region of IDT-BT (middle), and its power spectrum (right). The power spectrum shows an isotropic ring at a spatial frequency of $q \approx 0.4$ Å^{-1} corresponding to the (001) reflection of the backbone (i.e., along the chain). This power spectrum is nearly equivalent to the nanodiffraction patterns presented in Figure 1d. (b) Exploratory visualization of nanoscale features on a representative 100 nm × 100 nm region of IDT-BT. Expanded views of four bandpass-filtered 12.3 nm × 12.3 nm regions illustrate the polymer backbone arrangement and the presence of locally well-defined backbone stacking peaks. The bandpass filter is centered at $q \approx 0.4$ Å^{-1} ± 0.03 Å^{-1}. We note the lack of traditional, readily interpretable structural features often encountered in semicrystalline polymers, such as alkyl- and π-stacking, making it challenging to directly observe structural features associated with the backbone repeat. (c) Power spectrum (left) of the HRTEM image shown in part (b) and a lineout of an azimuthally integrated power spectrum (right). (d) Computed director field of the bottom right region of the image shown in part (b). (e) Reconstruction of the predominant polymer orientation extracted from the computed director field. In the director field map, short lines are drawn parallel to the direction of the observed backbone stacking peaks. These short lines are then propagated following the local slope taken from the director field to reconstruct the predominant polymer orientation map.

plane (q_{xy}) peaks at ≈0.4, 0.8, and 1.2 Å^{-1} assigned to the infrequently observed "backbone" reflections (00l), a feature associated with the polymer repeat unit length (≈1.56 nm). Something of a misnomer, these "backbone" reflections require precise intermolecular shifts of adjacent chains. These directions are generally thought to be "soft" since local tilting/slipping of neighboring chains can disrupt translational order. The series of narrow (00l) peaks is accompanied by a broad halo at ≈1.2−1.5 Å^{-1} attributed to diffraction from disordered side chains and comparatively weak and broad diffraction alkyl (200) and π-stacking (010) peaks with short coherence lengths and reduced crystallinity (Table S1).[47,49]

GIWAXS patterns suggest both edge-on and face-on populations in the bulk, in contrast with polarized near-edge X-ray spectroscopy measurements,[47] indicating a nearly perfect face-on texture in top and buried interfaces (~2 nm).[57] Scanning tunneling microscopy on submonolayer films shows that IDT-BT is capable, under certain processing conditions, of side-chain interdigitation and parallel alignment of local strands.[55] Furthermore, molecular dynamics simulations of the unit cell of IDT-BT predict side-chain interdigitation of adjacent lamellae.[49] These results suggest that traditional bulk X-ray diffraction or spectroscopy techniques fail to fully capture the nano- to mesoscale structure of materials lacking long-range order such as IDT-BT.

To further investigate mesoscale heterogeneity, we conducted FEL X-ray diffraction measurements using a "diffraction before destruction" methodology[58] to avoid X-ray damage (Figure 1d). Diffraction patterns of IDT-BT were captured by using a single, high-intensity X-ray pulse (≈100 fs) focused to ≈250 nm FWHM, each showing a sharp ring at ≈0.4 Å^{-1} and a broad halo at ≈1.2−1.5 Å^{-1}, matching well the observed features in GIWAXS (Figure 1c). The backbone ring (001) is mostly uniform with slight variations suggestive of a finite but large number of crystallites contributing without discernible local orientational order. There is some scattered intensity at q-values below the (001) peak; however, azimuthal integration of the data (Figure S3) does not show any feature resembling a

https://doi.org/10.1021/acsmacrolett.1c00547
ACS Macro Lett. 2021, 10, 1306−1314

peak that could be attributed to in-plane alkyl stacking of the polymer. The data suggest that the microstructure of IDT-BT must be probed at length scales significantly smaller than the size of the X-ray beam to enable assessment of the mesoscale heterogeneity.[59,60] Toward this end, we visualize the structure of IDT-BT with nanometer-scale resolution using low-dose cryogenic HRTEM.

With the electron beam at normal incidence, HRTEM can directly image in-plane diffracting features.[26,36] A schematic of the HRTEM imaging setup is shown in Figure 2a, where the imaging conditions (described in Sections 1 and 3, SI) are optimized to image the backbone lattice spacing of IDT-BT. In agreement with X-ray results, the computed power spectrum over a region of ≈200 nm in diameter (Figure 2a) shows a sharp diffraction ring related to the backbone repeat unit, indicating the presence of aligned backbone sections with overall isotropic orientation. A representative 100 nm × 100 nm region of IDT-BT, its computed power spectrum, and the computed power spectra from smaller subregions are shown in Figure 2b,c. Whereas the spectrum of the full region shows a continuous ring at ≈0.4 $Å^{-1}$, the spectra of individual 12 nm × 12 nm subregions exhibit discrete, well-defined peaks. Within these subregions, the backbone peak is spotty, suggesting relatively well-defined nanocrystalline domains that often overlap within the small windows. We note that while it is not possible to determine the order of the polymer along the beam direction (through the thickness of the film), given that we frequently observe overlapping structures, a number of layers are presumed to exist. Moreover, we are only probing nanocrystalline domains that have components that satisfy the Bragg condition, and some crystalline regions may not be imaged in this analysis, suggesting the degree of order is underestimated.

To better visualize the local alignment of IDT-BT and show the coupling of local chain aggregates from the nanoscale to mesoscale, we use digital image processing methods (Sections 3 and 4, SI) and resolve the local average molecular orientation over length scales ranging from nanometers to tens or hundreds of nanometers. We start by visualizing a small 50 nm × 50 nm image region of IDT-BT. The director field (Figure 2d) represents a spatial mapping of the average direction of the polymer backbones visible in the projected image, and it is composed of short lines drawn parallel to the backbone direction extracted from the computed power spectrum over small 12 nm × 12 nm regions of the film.[36] Brandley et al. have applied similar methods to map the orientation of carbon nanotubes from scanning electron micrographs.[61] We observe nanometer-scale regions of locally aligned polymer chains and frequent overlapping between regions. Using the local value of the molecular director as the tangent vector, lines representing the predominant orientation of the backbone are propagated to follow the slow contours of the director field map, as shown in Figure 2e. The reconstructed map of the polymer backbone orientation displays the presence of nanoscale domains of aligned polymer chains and overlapping of domains. We emphasize that these schematic images show the average likely direction of the polymer backbones. The complex local structure combined with the limited electron dose make single-chain imaging impractical. Similar features are observed through a reconstruction of the average polymer orientation along the backbone direction over larger length scales (Figure 3 and Figure S6). Whereas at short length scales (≲10 nm) the polymer is likely to be locally aligned and exhibit a well-defined orientation, over larger length scales (hundreds of nanometers), these regions of locally aligned backbones show an overall isotropic orientation.

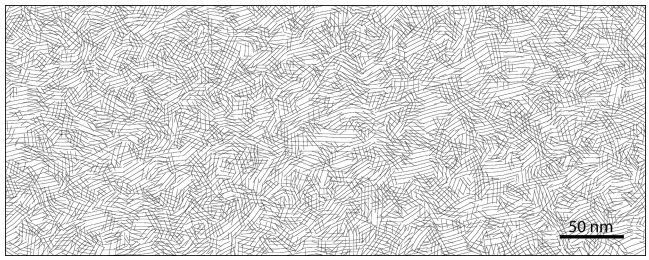

Figure 3. Reconstruction of the predominant backbone orientation based on an HRTEM image of IDT-BT. Small (≈10−20 nm) domains of aligned polymer chains are observed along with a highly overlapping structure.

Gathering statistical information about structural features such as domain size and grain boundaries is of interest for the interpretation of charge transport properties in conjugated polymers.[8,21] To characterize and quantify the extent of the nanoscale domains present in IDT-BT, we develop an algorithm to segment HRTEM images into neighboring regions with similar polymer alignment (within ±5°), and we identify them as single domains. This angle range is chosen to approximately match both the angular distribution of the locally averaged domains (*vide infra*) and an informative qualitative picture consistent with the level of disorder. As shown in Figure 4a, this method spatially identifies domains and overlaps between domains. Since larger domains will cover larger areas of the sample, we present the cumulative area-weighted distribution in Figure 4b. For half of the sampled area, the domains are ≳20 nm. The mean value of the area-weighted distribution (≈16 nm) agrees with the estimated coherence length (≈14 nm) from GIWAXS of the (001) peak using the Scherrer equation (Figure S10 and Table S1, respectively). The analysis of the grain boundary angles was performed by calculating the relative misorientation between one domain and neighboring or overlapping domains (Figure 4c). All grain boundary orientations are observed, with a preference for ≈20° and a slighter one for ≈90° grain boundaries. Further details are provided in Section 5, SI.

The domain analysis and segmentation process also offer new opportunities to examine order in macroscopically isotropic samples. Stiff, rod-like polymers can have both crystalline and liquid-crystalline-like phases.[21,62−64] Fast scanning calorimetry measurements of IDT-BT show two distinct endotherms upon annealing above the glass transition temperature, indicating possible liquid-crystalline or liquid-crystalline-like transitions.[64] This liquid-crystalline-like character is already apparent from the orientation maps (Figure 3); however, there may be additional weak and/or broad molecular features available. To investigate whether such features exist for the expected in-plane alkyl feature of face-on crystallites, we reorient the calculated power spectra of individually segmented domains to a common backbone orientation and compute the median (Figure S7). No significant diffraction or diffuse scattering signal is observed in the expected range of an alkyl peak (i.e., between 2−3 nm and approximately orthogonal to the backbone reflection), suggesting a lack of translational symmetry along the alkyl direction for face-on polymer regions and thus a liquid-

https://doi.org/10.1021/acsmacrolett.1c00547
ACS Macro Lett. 2021, 10, 1306−1314

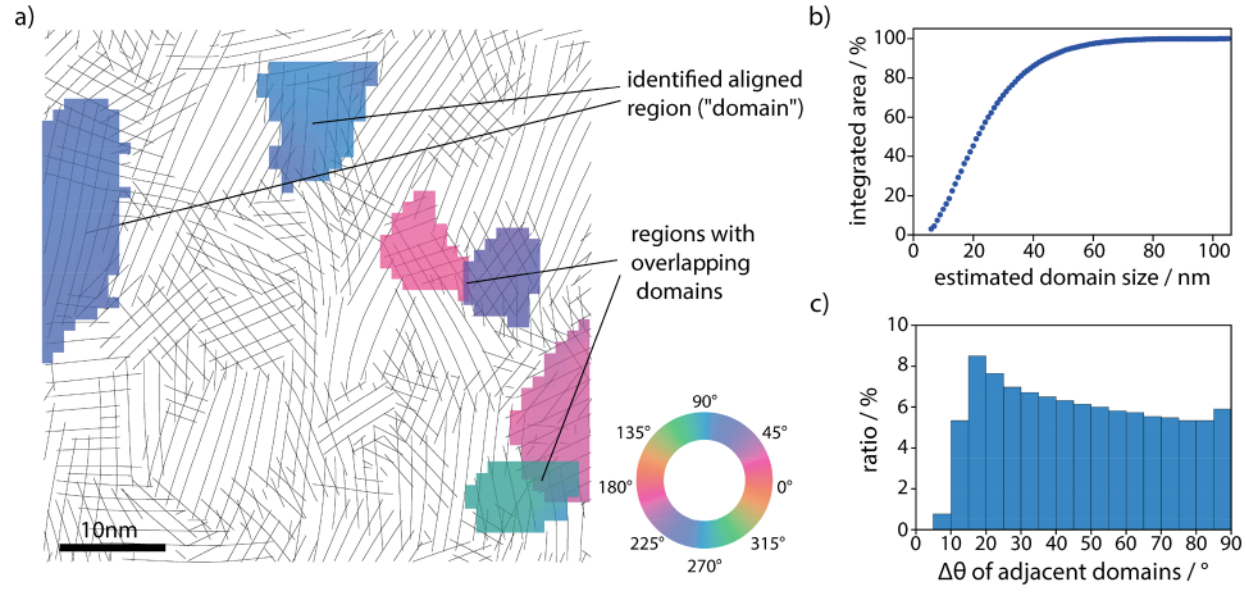

Figure 4. Domain identification and analysis. (a) Illustrative example of the clustering algorithm, which identifies and spatially segments an HRTEM image into regions ("domains") of aligned backbone within ±5°. The color of each domain is calculated from the median orientation of the identified domains. The map of identified domains is overlaid with the predominant polymer orientation map shown in Figure 2e for illustratory purposes. (b) Cumulative area-weighted distribution of domain sizes calculated across various HRTEM images, equivalent to a probed area of ≈9 μm^2. (c) Histogram showing the distribution of grain boundary misorientations.

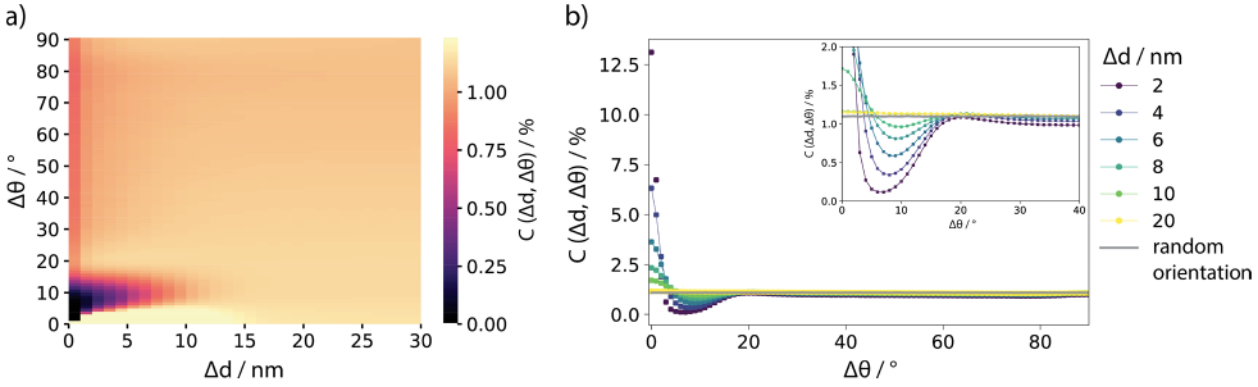

Figure 5. Local orientational spatial autocorrelation analysis over a probed area of ≈9 μm^2 of IDT-BT. (a) Heatmap of the local orientational autocorrelations, $C(\Delta d, \Delta\theta)$. The scaling range is computed using robust quantiles of $C(\Delta d, \Delta\theta)$ instead of the extreme values. (b) Extracted linecuts of $C(\Delta d, \Delta\theta)$ at selected distances (Δd). A representative linecut (at Δd = 20 nm) for a simulated sample with random backbone orientations is shown in gray. Extreme values were accounted for scaling of the y-axis. Inset: close-up view of extracted linectus of $C(\Delta d, \Delta\theta)$ for low $\Delta\theta$ values.

crystalline-like behavior.[47,49] The absence of an in-plane (100) peak in both the X-ray results (Figure 1) and the reoriented median power spectrum of the domains is interesting with several possible explanations. Whereas it is possible in some regions of the film that there exist face-on regions with side-chain interdigitation and the formation of compact assemblies,[55] we have yet to observe these in spin-coated thin films, suggesting these events are rare or exist primarily at the interface. If the face-on assumption of the planar polymer backbone is correct, it is possible that IDT-BT adopts an altogether different and unknown thin-film structure. This could include crossed-chain homoepitaxial motifs previously reported by Takacs et al.[24] and Schulz et al.,[25] quenched disorder of defects along the chain axis, or even liquid-crystalline phases. Alternatively, the domains may consist of edge-on crystallites.

Given that charge transport in conjugated polymers requires electronic connectivity across various length scales,[11] it is of interest to characterize the extended structural correlations in IDT-BT beyond the size of its domains. We choose a statistical measure that describes spatial relationships of how locally aligned domains change as a function of distance (Δd) and misorientation ($\Delta\theta$). The probability of finding two locally aligned regions of the polymer separated by Δd and $\Delta\theta$ follows the autocorrelation function

$$\cdots \frac{\cdot \cdots \cdot \cdots \cdot \cdots \cdot \cdots}{\cdot \cdots \cdot \cdots \cdot \cdots}$$

where $f(d, \theta)$ is a binary value indicating whether a backbone peak is present at (d, θ). Similarly, $f(d + \Delta d, \theta + \Delta\theta)$ is a binary value indicating whether there exists a backbone peak at a $(\Delta d, \Delta\theta)$ relative to $f(d, \theta)$. The denominator term, $\sum f(d) \times f(d + \Delta d)|_d$, is the sum of all backbone peaks separated by Δd.

https://doi.org/10.1021/acsmacrolett.1c00547
ACS Macro Lett. 2021, 10, 1306−1314

This normalization term accounts for the fact that some distances are more likely to occur than others on the analysis grid. To compare the observed structural correlations in IDT-BT relative to a sample not expected to present clustered regions of locally aligned backbones, the autocorrelations of a simulated sample with random backbone orientations were calculated (representative lineout shown in Figure 5b). Comparisons with IDT-BT are further discussed in Section 6 of the SI.

The heatmap of $C(\Delta d, \Delta\theta)$ and extracted linecuts for representative distances (Figure 5) highlight several structural features of interest. For $\Delta d \lesssim 10$ nm, we observe a prevalence for local alignment of IDT-BT within 5°, which is well in agreement with the median value of the domain size distribution (Section 5, SI). For $\Delta d \gtrsim 15$ nm, the autocorrelations of IDT-BT agree with the observed $C(\Delta d, \Delta\theta)$ values of the simulated sample with random orientations (Figure S11), indicating that correlations do not typically survive beyond ≈15 nm, and the material exhibits an isotropic behavior at these length scales. Importantly, for $\Delta d \lesssim 10$ nm, there is a lower than random probability for regions of aligned polymer chains to exhibit angular misorientations between ≈5 and 18°, suggesting an impediment for forming low-angle grain boundaries. Reminiscent of the observed preferential grain boundaries at ≈20° and 90° (Figure 4c), the heatmap z-score of the autocorrelations (Figure S12c,d) suggests increased likelihood for domain overlapping at these angles for $\Delta d \lesssim 10$ nm. Despite their weak signal, these features could have profound, nonlinear implications in domain interconnectivity.[24,65] We hypothesize these correlations originate from two possible structures. Given that HRTEM images represent a projection of the sample structure through the thickness of the film and that IDT-BT exhibits weak order along the π-stacking direction (Figure 1), it is possible that IDT-BT nanodomains are not tolerant to defects between layers and that attempts to stack result in a relative rotation between layers that likely maintain a common backbone reflection. Alternatively, defects along the chain axis that maintain backbone planarity, such as a rotation between the IDT and BT units, produce a curvature bend that locally changes the direction of the backbone.

Our work showcases the potential of low-dose cryogenic HRTEM and data analytics to advance our understanding of complex, functional soft matter. We have unveiled the nanoscale and mesoscale structure of a material often considered "amorphous-like", finding evidence for remarkable short- and medium-range order and unconventional packing structures relative to conventional semicrystalline polymers.[36] By mapping the backbone spacing reflection, we have identified nanometer-scale regions of locally aligned polymer chains (domains) yet found no evidence for alkyl stacking in these ordered phases, suggesting that solution-processed films of IDT-BT exhibit aspects of liquid-crystalline behavior. Analysis of the local orientational spatial autocorrelations suggests that IDT-BT forms packing structures of domains at preferential overlapping angles, which might affect electronic transport properties. Charge transport in conjugated polymers depends on molecular structure, chain conformation, local aggregation, and mesoscale order. While chain rigidity is an important factor in limiting energetic disorder,[49] it also likely contributes to the development of the nanoscale and mesoscale order we observe by HRTEM. The coexistence of charge delocalization along the rigid backbone favored by the molecular structure and an advantageous mesostructure featuring medium-range order are instrumental in enabling the outstanding charge transport properties of IDT-BT.

This study showcases the applicability of using HRTEM to characterize the rich, complex mesoscale structure of conjugated polymers with unprecedented detail, shedding light on the pitfalls of using conventional descriptors of order and bulk characterization techniques to elucidate the complex microstructure of materials lacking long-range order and overt crystallinity yet exhibiting outstanding molecular order.

ASSOCIATED CONTENT

Supporting Information

The Supporting Information is available free of charge at https://pubs.acs.org/doi/10.1021/acsmacrolett.1c00547.

Experimental methods, DFT-optimized structures of linear chains, and further details about the digital image processing methods (PDF)

AUTHOR INFORMATION

Corresponding Authors

Alberto Salleo − *Department of Materials Science and Engineering, Stanford University, Stanford, California 94305, United States*; Email: asalleo@stanford.edu

Christopher J. Takacs − *Stanford Synchrotron Radiation Lightsource, SLAC National Accelerator Laboratory, Menlo Park, California 94025, United States*; Email: ctakacs@slac.stanford.edu

Authors

Camila Cendra − *Department of Materials Science and Engineering, Stanford University, Stanford, California 94305, United States*; orcid.org/0000-0003-1786-6540

Luke Balhorn − *Department of Materials Science and Engineering, Stanford University, Stanford, California 94305, United States*

Weimin Zhang − *Physical Science and Engineering Division KAUST Solar Center (KSC), King Abdullah University of Science and Technology (KAUST), Thuwal 23955-6900, Saudi Arabia*

Kathryn O'Hara − *Materials Department, University of California• Santa Barbara, Santa Barbara, California 93106, United States*

Karsten Bruening − *Stanford Synchrotron Radiation Lightsource, SLAC National Accelerator Laboratory, Menlo Park, California 94025, United States*

Christopher J. Tassone − *Stanford Synchrotron Radiation Lightsource, SLAC National Accelerator Laboratory, Menlo Park, California 94025, United States*

Hans-Georg Steinrueck − *Stanford Synchrotron Radiation Lightsource, SLAC National Accelerator Laboratory, Menlo Park, California 94025, United States; Department Chemie, Universität Paderborn, 33098 Paderborn, Germany;* orcid.org/0000-0001-6373-0877

Mengning Liang − *Stanford Synchrotron Radiation Lightsource, SLAC National Accelerator Laboratory, Menlo Park, California 94025, United States*

Michael F. Toney − *Stanford Synchrotron Radiation Lightsource, SLAC National Accelerator Laboratory, Menlo Park, California 94025, United States; Department of Chemical and Biological Engineering, University of Colorado• Boulder, Boulder, Colorado 80303, United States;* orcid.org/0000-0002-7513-1166

Iain McCulloch − *Physical Science and Engineering Division KAUST Solar Center (KSC), King Abdullah University of Science and Technology (KAUST), Thuwal 23955-6900, Saudi Arabia; Department of Chemistry, University of Oxford, Oxford OX1 3TA, United Kingdom*

Michael L. Chabinyc − *Materials Department, University of California• Santa Barbara, Santa Barbara, California 93106, United States;* orcid.org/0000-0003-4641-3508

Complete contact information is available at: https://pubs.acs.org/10.1021/acsmacrolett.1c00547

Author Contributions

The manuscript was written through contributions of all authors. All authors have given approval to the final version of the manuscript.

Notes

The authors declare no competing financial interest.

ACKNOWLEDGMENTS

We thank Dr. Elizabeth Montabana, Dr. David Buschnell, and Dr. Dong-Hua Chen for technical assistance with the Tecnai F20 transmission electron microscope. We also thank Dr. Sébastien Boutet at the Linac Coherent Light Source (LCLS) for FEL beamline assistance. Work by C.C. and L.B. on image analysis was supported by the U.S. Department of Energy (DOE), Office of Science, Basic Energy Sciences (BES) under Award DE-SC0020046. C.C. and A.S. also gratefully acknowledge financial support from the National Science Foundation Award # DMR 1808401. C.J.T., K.O., and M.L.C. also acknowledge financial support from the National Science Foundation Award # DMR 1436263. We also gratefully acknowledge the support of NVIDIA Corporation with the donation of the Titan V GPU used for this research. Some of this work was performed at the Stanford-SLAC Cryo-EM Facilities, supported by Stanford University, SLAC, and the National Institutes of Health S10 Instrumentation Programs. Measurements at Stanford Synchrotron Radiation Lightsource, SLAC National Accelerator Laboratory, were supported by the U.S. Department of Energy, Office of Science, Office of Basic Energy Sciences under Contract No. DE-AC02-76SF00515. Use of the Linac Coherent Light Source (LCLS), SLAC National Accelerator Laboratory, is supported by the U.S. Department of Energy, Office of Science, Office of Basic Energy Sciences under Contract No. DE-AC02-76SF00515.

REFERENCES

(1) Fan, Q.; Su, W.; Chen, S.; Kim, W.; Chen, X.; Lee, B.; Liu, T.; Méndez-Romero, U. A.; Ma, R.; Yang, T.; Zhuang, W.; Li, Y.; Li, Y.; Kim, T. S.; Hou, L.; Yang, C.; Yan, H.; Yu, D.; Wang, E. Mechanically Robust All-Polymer Solar Cells from Narrow Band Gap Acceptors with Hetero-Bridging Atoms. *Joule* **2020**, *4* (3), 658−672.

(2) Huitema, H. E. A.; Gelinck, G. H.; Van Der Putten, J. B. P. H.; Kuijk, K. E.; Hart, C. M.; Cantatore, E.; De Leeuw, D. M. Active-Matrix Displays Driven by Solution Processed Polymeric Transistors. *Adv. Mater.* **2002**, *14* (17), 1201−1204.

(3) Moia, D.; Giovannitti, A.; Szumska, A. A.; Maria, I. P.; Rezasoltani, E.; Sachs, M.; Schnurr, M.; Barnes, P. R. F. F.; McCulloch, I.; Nelson, J. Design and Evaluation of Conjugated Polymers with Polar Side Chains as Electrode Materials for Electrochemical Energy Storage in Aqueous Electrolytes. *Energy Environ. Sci.* **2019**, *12* (4), 1349−1357.

(4) Parlak, O.; Keene, S. T.; Marais, A.; Curto, V. F.; Salleo, A. Molecularly Selective Nanoporous Membrane-Based Wearable Organic Electrochemical Device for Noninvasive Cortisol Sensing. *Sci. Adv.* **2018**, *4* (7), eaar2904.

(5) Chen, Y.; Rommelfanger, N. J.; Mahdi, A. I.; Wu, X.; Keene, S. T.; Obaid, A.; Salleo, A.; Wang, H.; Hong, G. How Is Flexible Electronics Advancing Neuroscience Research? *Biomaterials* **2021**, *268*, 120559.

(6) Melianas, A.; Quill, T. J.; LeCroy, G.; Tuchman, Y.; Loo, H. V.; Keene, S. T.; Giovannitti, A.; Lee, H. R.; Maria, I. P.; McCulloch, I.; Salleo, A. Temperature-Resilient Solid-State Organic Artificial Synapses for Neuromorphic Computing. *Sci. Adv.* **2020**, *6* (27), 1−8.

(7) Patel, S.; Glaudell, A.; Peterson, K.; Thomas, E.; O'Hara, K.; Lim, E.; Chabinyc, M.; Oschmann, B.; Lawrence, J.; Schulze, M. W.; Ren, J. M.; Anastasaki, A.; Luo, Y.; Nothling, M. D.; Pester, C. W.; Delaney, K. T.; Connal, L. A.; McGrath, A. J.; Clark, P. G.; Bates, C. M.; Hawker, C. J. Morphology Controls the Thermoelectric Power Factor of a Doped Semiconducting Polymer. *Sci. Adv.* **2017**, *3* (6), e1700434.

(8) Salleo, A.; Kline, R. J.; DeLongchamp, D. M.; Chabinyc, M. L. Microstructural Characterization and Charge Transport in Thin Films of Conjugated Polymers. *Adv. Mater.* **2010**, *22* (34), 3812−3838.

(9) Liu, T.; Troisi, A. Understanding the Microscopic Origin of the Very High Charge Mobility in PBTTT: Tolerance of Thermal Disorder. *Adv. Funct. Mater.* **2014**, *24* (7), 925−933.

(10) Spakowitz, A. J. Polymer Physics across Scales: Modeling the Multiscale Behavior of Functional Soft Materials and Biological Systems. *J. Chem. Phys.* **2019**, *151* (23), 230902.

(11) Mollinger, S. A.; Krajina, B. A.; Noriega, R.; Salleo, A.; Spakowitz, A. J. Percolation, Tie-Molecules, and the Microstructural Determinants of Charge Transport in Semicrystalline Conjugated Polymers. *ACS Macro Lett.* **2015**, *4* (7), 708−712.

(12) Raabe, D.; Godara, A. Mesoscale Simulation of the Kinetics and Topology of Spherulite Growth during Crystallization of Isotactic Polypropylene (IPP) by Using a Cellular Automaton. *Modell. Simul. Mater. Sci. Eng.* **2005**, *13* (5), 733−751.

(13) Khoury, F. The Spherulitic Crystallization of Isotactic Polypropylene From Solution : On the Evolution of Monoclinic Spherulites From Dendritic Chain-Folder Crystal Precursors. *J. Res. Natl. Bur. Stand., Sect. A* **1966**, *70A* (1), 29−61.

(14) Panova, O.; Chen, X. C.; Bustillo, K. C.; Ophus, C.; Bhatt, M. P.; Balsara, N.; Minor, A. M. Orientation Mapping of Semicrystalline Polymers Using Scanning Electron Nanobeam Diffraction. *Micron* **2016**, *88*, 30−36.

(15) Panova, O.; Ophus, C.; Takacs, C. J.; Bustillo, K. C.; Balhorn, L.; Salleo, A.; Balsara, N.; Minor, A. M. Diffraction Imaging of Nanocrystalline Structures in Organic Semiconductor Molecular Thin Films. *Nat. Mater.* **2019**, *18*, 860.

(16) Knaapila, M.; Bright, D. W.; Stepanyan, R.; Torkkeli, M.; Almásy, L.; Schweins, R.; Vainio, U.; Preis, E.; Galbrecht, F.; Scherf, U.; Monkman, A. P.; Alm, L.; Schweins, R.; Vainio, U.; Preis, E.; Galbrecht, F.; Scherf, U.; Monkman, A. P. Network Structure of Polyfluorene Sheets as a Function of Alkyl Side Chain Length. *Phys. Rev. E - Stat. Nonlinear, Soft Matter Phys.* **2011**, *83* (5), 1−11.

(17) Knaapila, M.; Dias, F. B.; Garamus, V. M.; Almásy, L.; Torkkeli, M.; Leppänen, K.; Galbrecht, F.; Preis, E.; Burrows, H. D.; Scherf, U.; Monkman, A. P. Influence of Side Chain Length on the Self-Assembly of Hairy-Rod Poly(9,9-Dialkylfluorene)s in the Poor Solvent Methylcyclohexane. *Macromolecules* **2007**, *40* (26), 9398−9405.

(18) Chen, S. H.; Chou, H. L.; Su, A. C.; Chen, S. A. Molecular Packing in Crystalline Poly(9,9-Di-n-Octyl-2,7-Fluorene). *Macromolecules* **2004**, *37* (18), 6833−6838.

(19) Gujral, A.; O'Hara, K. A.; Toney, M. F.; Chabinyc, M. L.; Ediger, M. D. Structural Characterization of Vapor-Deposited Glasses of an Organic Hole Transport Material with X-Ray Scattering. *Chem. Mater.* **2015**, *27* (9), 3341−3348.

(20) Wood, B. A.; Thomas, E. L. Are Domains in Liquid Crystalline Polymers Arrays of Disclinations? *Nature* **1986**, *324* (6098), 655−657.

(21) Zhang, X.; Hudson, S. D.; Delongchamp, D. M.; Gundlach, D. J.; Heeney, M.; McCulloch, I. In-Plane Liquid Crystalline Texture of

High-Performance Thienothiophene Copolymer Thin Films. *Adv. Funct. Mater.* **2010**, *20* (23), 4098−4106.
(22) Hudson, S. D.; Lovinger, A. J.; Gomez, M. A.; Lorente, J.; Marco, C.; Fatou, J. G. Relationship between Mesophase and Semicrystalline Morphology in Smectic Liquid Crystalline Polymers. *Macromolecules* **1994**, *27* (12), 3357−3362.
(23) Kim, B. G.; Jeong, E. J.; Chung, J. W.; Seo, S.; Koo, B.; Kim, J. A Molecular Design Principle of Lyotropic Liquid-Crystalline Conjugated Polymers with Directed Alignment Capability for Plastic Electronics. *Nat. Mater.* **2013**, *12* (7), 659−664.
(24) Takacs, C. J.; Brady, M. A.; Treat, N. D.; Kramer, E. J.; Chabinyc, M. L. Quadrites and Crossed-Chain Crystal Structures in Polymer Semiconductors. *Nano Lett.* **2014**, *14* (6), 3096−3101.
(25) Schulz, G. L.; Fischer, F. S. U.; Trefz, D.; Melnyk, A.; Hamidi-Sakr, A.; Brinkmann, M.; Andrienko, D.; Ludwigs, S. The PCPDTBT Family: Correlations between Chemical Structure, Polymorphism, and Device Performance. *Macromolecules* **2017**, *50* (4), 1402−1414.
(26) Martin, D. C.; Thomas, E. L. Grain Boundaries in Extended-Chain Polymers: Theory and Experiment. *Philos. Mag. A* **1991**, *64* (4), 903−922.
(27) Bustillo, K. C.; Panova, O.; Chen, X. C.; Takacs, C. J.; Ciston, J.; Ophus, C.; Balsara, N. P.; Minor, A. M. Nanobeam Scanning Diffraction for Orientation Mapping of Polymers. *Microsc. Microanal.* **2017**, *23* (S1), 1782−1783.
(28) Noriega, R.; Rivnay, J.; Vandewal, K.; Koch, F. P. V.; Stingelin, N.; Smith, P.; Toney, M. F.; Salleo, A. A General Relationship between Disorder, Aggregation and Charge Transport in Conjugated Polymers. *Nat. Mater.* **2013**, *12* (11), 1038−1044.
(29) Noriega, R. Efficient Charge Transport in Disordered Conjugated Polymer Microstructures. *Macromol. Rapid Commun.* **2018**, *39* (14), 1800096.
(30) Zhang, X.; Richter, L. J.; Delongchamp, D. M.; Kline, R. J.; Hammond, M. R.; McCulloch, I.; Heeney, M.; Ashraf, R. S.; Smith, J. N.; Anthopoulos, T. D.; Schroeder, B.; Geerts, Y. H.; Fischer, D. A.; Toney, M. F. Molecular Packing of High-Mobility Diketo Pyrrolo-Pyrrole Polymer Semiconductors with Branched Alkyl Side Chains. *J. Am. Chem. Soc.* **2011**, *133* (38), 15073−15084.
(31) Kübel, C.; González-Ronda, L.; Drummy, L. F.; Martin, D. C. Defect-Mediated Curvature and Twisting in Polymer Crystals. *J. Phys. Org. Chem.* **2000**, *13* (12), 816−829.
(32) Takacs, C. J.; Sun, Y.; Welch, G. C.; Perez, L. A.; Liu, X.; Wen, W.; Bazan, G. C.; Heeger, A. J. Solar Cell Efficiency, Self-Assembly, and Dipole-Dipole Interactions of Isomorphic Narrow-Band-Gap Molecules. *J. Am. Chem. Soc.* **2012**, *134* (40), 16597−16606.
(33) Sun, Y.; Welch, G. C.; Leong, W. L.; Takacs, C. J.; Bazan, G. C.; Heeger, A. J. Solution-Processed Small-Molecule Solar Cells with 6.7% Efficiency. *Nat. Mater.* **2012**, *11* (1), 44−48.
(34) Voyles, P.; Hwang, J. Fluctuation Electron Microscopy. *Charact. Mater.* **2012**, DOI: 10.1002/0471266965.com138.
(35) O'Hara, K.; Takacs, C. J.; Liu, S.; Cruciani, F.; Beaujuge, P.; Hawker, C. J.; Chabinyc, M. L. Effect of Alkyl Side Chains on Intercrystallite Ordering in Semiconducting Polymers. *Macromolecules* **2019**, *52* (7), 2853−2862.
(36) Takacs, C. J.; Treat, N. D.; Krämer, S.; Chen, Z.; Facchetti, A.; Chabinyc, M. L.; Heeger, A. J. Remarkable Order of a High-Performance Polymer. *Nano Lett.* **2013**, *13* (6), 2522−2527.
(37) Love, J. A.; Nagao, I.; Huang, Y.; Kuik, M.; Gupta, V.; Takacs, C. J.; Coughlin, J. E.; Qi, L.; Van Der Poll, T. S.; Kramer, E. J.; Heeger, A. J.; Nguyen, T. Q.; Bazan, G. C. Silaindacenodithiophene-Based Molecular Donor: Morphological Features and Use in the Fabrication of Compositionally Tolerant, High-Efficiency Bulk Heterojunction Solar Cells. *J. Am. Chem. Soc.* **2014**, *136* (9), 3597−3606.
(38) Martin, D. C.; Chen, J.; Yang, J.; Drummy, L. F.; Kübel, C. High Resolution Electron Microscopy of Ordered Polymers and Organic Molecular Crystals: Recent Developments and Future Possibilities. *J. Polym. Sci., Part B: Polym. Phys.* **2005**, *43* (14), 1749−1778.
(39) Martin, D. C.; Thomas, E. L. Experimental High-Resolution Electron Microscopy of Polymers. *Polymer* **1995**, *36* (9), 1743−1759.
(40) Martin, D. C.; Thomas, E. L. Ultrastructure of Poly(b-Phenylenebenzobisoxazole) Fibers. *Macromolecules* **1991**, *24*, 2450−2460.
(41) Stratton, W. G.; Hamann, J.; Perepezko, J. H.; Voyles, P. M.; Mao, X.; Khare, S. V. Aluminum Nanoscale Order in Amorphous Al92 Sm8Measured by Fluctuation Electron Microscopy. *Appl. Phys. Lett.* **2005**, *86* (14), 141910.
(42) Gibson, J. M.; Treacy, M. M. J.; Sun, T.; Zaluzec, N. J. Substantial Crystalline Topology in Amorphous Silicon. *Phys. Rev. Lett.* **2010**, *105* (12), 1−4.
(43) Yang, Y.; Zhou, J.; Zhu, F.; Chang, D.; Kim, D. S.; Yuan, Y.; Pham, M.; Rana, A.; Tian, X.; Yao, Y.; Osher, S.; Hu, L.; Ercius, P.; Miao, J. Determining the Three-Dimensional Atomic Structure of an Amorphous Solid. *Nature* **2021**, *592*, 60.
(44) Glaeser, R. M.; McMullan, G.; Faruqi, A. R.; Henderson, R. Images of Paraffin Monolayer Crystals with Perfect Contrast: Minimization of Beam-Induced Specimen Motion. *Ultramicroscopy* **2011**, *111* (2), 90−100.
(45) Shigematsu, H.; Sigworth, F. J. Noise Models and Cryo-EM Drift Correction with a Direct-Electron Camera. *Ultramicroscopy* **2013**, *131*, 61−69.
(46) Henderson, R. From Electron Crystallography to Single Particle CryoEM (Nobel Lecture). *Angew. Chem., Int. Ed.* **2018**, *57* (34), 10804−10825.
(47) Zhang, X.; Bronstein, H.; Kronemeijer, A. J.; Smith, J.; Kim, Y.; Kline, R. J.; Richter, L. J.; Anthopoulos, T. D.; Sirringhaus, H.; Song, K.; Heeney, M.; Zhang, W.; McCulloch, I.; Delongchamp, D. M. Molecular Origin of High Field-Effect Mobility in an Indacenodithiophene- Benzothiadiazole Copolymer. *Nat. Commun.* **2013**, *4*, 1−9.
(48) Zhang, W.; Smith, J.; Watkins, S. E.; Gysel, R.; McGehee, M.; Salleo, A.; Kirkpatrick, J.; Ashraf, S.; Anthopoulos, T.; Heeney, M.; McCulloch, I. Indacenodithiophene Semiconducting Polymers for High-Performance, Air-Stable Transistors. *J. Am. Chem. Soc.* **2010**, *132* (33), 11437−11439.
(49) Venkateshvaran, D.; Nikolka, M.; Sadhanala, A.; Lemaur, V.; Zelazny, M.; Kepa, M.; Hurhangee, M.; Kronemeijer, A. J.; Pecunia, V.; Nasrallah, I.; Romanov, I.; Broch, K.; McCulloch, I.; Emin, D.; Olivier, Y.; Cornil, J.; Beljonne, D.; Sirringhaus, H. Approaching Disorder-Free Transport in High-Mobility Conjugated Polymers. *Nature* **2014**, *515* (7527), 384−388.
(50) Lamport, Z. A.; Barth, K. J.; Lee, H.; Gann, E.; Engmann, S.; Chen, H.; Guthold, M.; McCulloch, I.; Anthony, J. E.; Richter, L. J.; DeLongchamp, D. M.; Jurchescu, O. D. A Simple and Robust Approach to Reducing Contact Resistance in Organic Transistors. *Nat. Commun.* **2018**, DOI: 10.1038/s41467-018-07388-3.
(51) Wadsworth, A.; Chen, H.; Thorley, K. J.; Cendra, C.; Nikolka, M.; Bristow, H.; Moser, M.; Salleo, A.; Anthopoulos, T. D.; Sirringhaus, H.; McCulloch, I. Modification of Indacenodithiophene-Based Polymers and Its Impact on Charge Carrier Mobility in Organic Thin-Film Transistors. *J. Am. Chem. Soc.* **2020**, *142* (2), 652−664.
(52) Thomas, T. H.; Harkin, D. J.; Gillett, A. J.; Lemaur, V.; Nikolka, M.; Sadhanala, A.; Richter, J. M.; Armitage, J.; Chen, H.; McCulloch, I.; Menke, S. M.; Olivier, Y.; Beljonne, D.; Sirringhaus, H. Short Contacts between Chains Enhancing Luminescence Quantum Yields and Carrier Mobilities in Conjugated Copolymers. *Nat. Commun.* **2019**, DOI: 10.1038/s41467-019-10277-y.
(53) Thomas, T. H.; Rivett, J. P. H.; Gu, Q.; Harkin, D. J.; Richter, J. M.; Sadhanala, A.; Yong, C. K.; Schott, S.; Broch, K.; Armitage, J.; Gillett, A. J.; Menke, S. M.; Rao, A.; Credgington, D.; Sirringhaus, H. Chain Coupling and Luminescence in High-Mobility, Low-Disorder Conjugated Polymers. *ACS Nano* **2019**, *13*, 13716.
(54) Kline, R. J.; DeLongchamp, D. M.; Fischer, D. A.; Lin, E. K.; Richter, L. J.; Chabinyc, M. L.; Toney, M. F.; Heeney, M.; McCulloch, I. Critical Role of Side-Chain Attachment Density on the Order and Device Performance of Polythiophenes. *Macromolecules* **2007**, *40* (22), 7960−7965.

https://doi.org/10.1021/acsmacrolett.1c00547
ACS Macro Lett. 2021, 10, 1306−1314

(55) Chen, H.; Wadsworth, A.; Ma, C.; Nanni, A.; Zhang, W.; Nikolka, M.; Luci, A. M. T.; Perdigão, L. M. A.; Thorley, K. J.; Cendra, C.; Larson, B.; Rumbles, G.; Anthopoulos, T. D.; Salleo, A.; Costantini, G.; Sirringhaus, H.; McCulloch, I. The Effect of Ring Expansion in Thienobenzo[b]Indacenodithiophene Polymers for Organic Field-Effect Transistors. *J. Am. Chem. Soc.* **2019**, *141* (47), 18806−18813.
(56) Zhang, W.; Gomez, E. D.; Milner, S. T. Predicting Chain Dimensions of Semiflexible Polymers from Dihedral Potentials. *Macromolecules* **2014**, *47* (18), 6453−6461.
(57) Sohn, K. E.; Dimitriou, M. D.; Genzer, J.; Fischer, D. A.; Hawker, C. J.; Kramer, E. J. Determination of the Electron Escape Depth for NEXAFS Spectroscopy. *Langmuir* **2009**, *25* (11), 6341−6348.
(58) Neutze, R.; Wouts, R.; Van Der Spoel, D.; Weckert, E.; Hajdu, J. Potential for Biomolecular Imaging with Femtosecond X-Ray Pulses. *Nature*; Macmillan Magazines Ltd.; August 17, 2000; pp 752−757. DOI: 10.1038/35021099.
(59) Gutt, C.; Grodd, L.; Mikayelyan, E.; Pietsch, U.; Kline, R. J.; Grigorian, S. Local Orientational Structure of a P3HT π-π Conjugated Network Investigated by X-Ray Nanodiffraction. *J. Phys. Chem. Lett.* **2014**, *5* (13), 2335−2339.
(60) Kurta, R. P.; Grodd, L.; Mikayelyan, E.; Gorobtsov, O. Y.; Zaluzhnyy, I. A.; Fratoddi, I.; Venditti, I.; Russo, M. V.; Sprung, M.; Vartanyants, I. A.; Grigorian, S. Local Structure of Semicrystalline P3HT Films Probed by Nanofocused Coherent X-Rays. *Phys. Chem. Chem. Phys.* **2015**, *17* (11), 7404−7410.
(61) Brandley, E.; Greenhalgh, E. S.; Shaffer, M. S. P.; Li, Q. Mapping Carbon Nanotube Orientation by Fast Fourier Transform of Scanning Electron Micrographs. *Carbon* **2018**, *137*, 78−87.
(62) Kuei, B.; Gomez, E. D. Chain Conformations and Phase Behavior of Conjugated Polymers. *Soft Matter* **2017**, *13* (1), 49−67.
(63) Chabinyc, M. L.; Toney, M. F.; Kline, R. J.; McCulloch, I.; Heeney, M. X-Ray Scattering Study of Thin Films of Poly(2,5-Bis(3-Alkylthiophen-2-Yl) Thieno[3,2-b]Thiophene). *J. Am. Chem. Soc.* **2007**, *129* (11), 3226−3237.
(64) Sommerville, P. J. W.; Li, Y.; Dong, B. X.; Zhang, Y.; Onorato, J. W.; Tatum, W. K.; Balzer, A. H.; Stingelin, N.; Patel, S. N.; Nealey, P. F.; Luscombe, C. K. Elucidating the Influence of Side-Chain Circular Distribution on the Crack Onset Strain and Hole Mobility of Near-Amorphous Indacenodithiophene Copolymers. *Macromolecules* **2020**, *53*, 7511.
(65) Takacs, C. J.; Collins, S. D.; Love, J. A.; Mikhailovsky, A. A.; Wynands, D.; Bazan, G. C.; Nguyen, T. Q.; Heeger, A. J. Mapping Orientational Order in a Bulk Heterojunction Solar Cell with Polarization-Dependent Photoconductive Atomic Force Microscopy. *ACS Nano* **2014**, *8* (8), 8141−8151.

https://doi.org/10.1021/acsmacrolett.1c00547
ACS Macro Lett. 2021, 10, 1306−1314